Ab Initio Evidence for Strong Correlation Associated with Mott Proximity in Iron-Based Superconductors

Takahiro Misawa, Kazuma Nakamura, and Masatoshi Imada

Department of Applied Physics, University of Tokyo, and JST CREST, 7-3-1 Hongo, Bunkyo-ku, Tokyo, 113-8656, Japan

(Received 18 December 2011; published 27 April 2012)

We predict that iron-based superconductors discovered near d^6 configuration (5 Fe 3d orbitals filled by 6 electrons) is located on the foot of an unexpectedly large dome of correlated electron matter centered at the Mott insulator at d^5 (namely, half filling). This is based on the many-variable variational Monte Carlo results for *ab initio* low-energy models derived by the downfolding. The d^5 Mott proximity extends to subsequent emergence of incoherent metals, orbital differentiations due to the Mott physics, and Hund's rule coupling, followed by antiferromagnetic quantum criticality, in quantitative accordance with available experiments.

DOI: 10.1103/PhysRevLett.108.177007 PACS numbers: 74.70.Xa, 71.27.+a, 71.30.+h, 74.20.Pq

Introduction.—Iron-based superconductors discovered in 2008 [1] soon proved to encompass different families of pnictides such as LaFeAsO and $BaFe_2As_2$ and chalcogenides such as FeSe and FeTe, where the superconductivity was discovered mostly under electron or hole doping as in the cuprate superconductors [2]. The backbone lattices are commonly built from a stacking of iron square-lattice layers. The band structures consisting mainly of the Fe 3d orbitals located near the Fermi level are also similar among the families [3]. However, physical properties strongly depend on the families and have a diversity in magnetic, transport, and superconducting properties [4].

The antiferromagnetic (AF) order is, in most cases, found close to the superconductivity, while the ordered magnetic moment has a diversity from zero up to $\geq 2\mu_B$ [5–8] whose origin is not entirely clear. Another diversity is found in the coherence of the metallic carrier. The incoherent (''bad metallic'') conduction with small Drude weight [9–12], enhanced mass in de Haas–van Alphen measurement [13], strongly renormalized quasiparticle peak in ARPES [14], unconventional AF fluctuations [15], and a typical Mott-Hubbard splitting (emergence of the lower Hubbard band) [16] have been claimed in several compounds, while the correlation effects are less clear in other cases [17,18]. Such a rich diversity is characteristic in contrast to the cuprate superconductors, in which strong correlation effects are common and universal. In this Letter, we first show that the diversity emerges indeed from the variation in the electron correlation.

The strength of electron correlation in the present materials is presently under hot debate partly because of this diversity. Firm and accurate calculations with full account of not only dynamical but also spatial fluctuation effects are desired. However, *ab initio* analyses with full account of spatial correlation effects require demanding calculations and to our knowledge are very few [19,20].

In this Letter, we employ an *ab initio* method [19] by a hybrid combination of density functional theory with accurate solvers for the downfolded effective low-energy model. Here, we employ the many-variable variational Monte Carlo (MVMC) method [21,22] for the solver. See [23], S.1 and S.3, for details of the whole method. The method enables us to examine strong correlation effects in an *ab initio* way fully with dynamical as well as spatial fluctuation effects. We find that the real iron-based superconductors are on the foot of a large dome structure centered around the d^5 Mott insulator, whose proximity effects generate various correlation phenomena of the real superconductors. This sheds new light on the understanding of the electron correlation effects in the iron-based materials.

In general, to vary and control electronic properties in correlated electron systems, two important routes are known [24]. One is the bandwidth (or equivalently effective-Coulomb-interaction) control and the other is the filling control. The former directly controls the ratio between the kinetic and interaction energies of electrons, while the latter tunes the distance from the ''commensurate filling'' (a simple fractional number of band filling enhances the electron correlation as in the Mott insulator). We show that both play key roles in the iron-based superconductors.

Model.—The derived *ab initio* parameters for the present effective models by the downfolding procedure [3,25] of the Fe 3d orbitals consist of the transfer integrals $t_{i,j,\nu,\mu}$ of an electron between the orbital ν on the site i, and μ on j, together with the orbital-dependent onsite direct-Coulomb ($U_{\nu,\mu}$) and the exchange ($J_{\nu,\mu}$) interactions. The ratio of the effective interactions (so called U representing the orbital average of $U_{\nu,\mu}$) to the bandwidth (or averaged transfer t) substantially (approximately 50%) increases in the order from LaFePO, LaFeAsO, $BaFe_2As_2$, FeTe to FeSe [3]. This is physically well understood by the increasing distance h between an iron layer and the neighboring pnictogen or chalcogen atoms, which alters the chemical bonding of the Fe 3d Wannier orbitals with the pnictogen

or chalcogen p orbitals from more covalent to more ionic in this order. This makes the Fe $3d$ Wannier orbitals more localized and the screening by pnictogen or chalcogen p and other orbitals less effective. Therefore, the family dependence offers a good example of the interaction control.

The interaction $U_{\mu,\nu}$ strongly depends on the orbitals μ, ν, and compounds. Nevertheless, all the derived *ab initio* models are reasonably well reproduced from that of a particular compound, say LaFeAsO, by a single parameter λ which scales all the interactions, $U_{\nu,\mu}$ and $J_{\nu,\mu}$, uniformly (see [23], S.2). In fact, λ is a measure of the electron correlation.

Result.—In Fig. 1(a), we show the ordered magnetic moment of the AF order $m(q_{\rm peak})$ (red circles) as a function of λ, calculated by MVMC method with the extrapolation to the thermodynamic limit. Here, $\lambda = 1$ represents the *ab initio* model for LaFeAsO, while by uniformly scaling all the interaction strength by λ without changing transfers except for orbital levels (see [23], S.1), the interaction control is monitored. We also plot the MVMC result of the real *ab initio* models for LaFePO, $BaFe_2As_2$, and FeTe, as black-framed yellow diamonds, at corresponding λ values (see [23], S.2) [22]. We note that we have derived and solved the 2D *ab initio* models for the first time here for the 4 compounds. On the other hand, in the previous study [22], we have treated the *ab initio* model only for LaFeAsO and only after a uniform scaling of both the interaction parameters for the dimensional downfolding and the La $4f$ screening, by using the downfolded model derived in Ref. [26]. The result for the *ab initio* models of FeTe shows the double-stripe order degenerate with the simple stripe with a nearly equal ordered moment. All the other results shown here indicate the stripe-ordered ground states. The agreement with the experimental results with the correct AF quantum critical point proves the accuracy of the present scheme. Similar quantitative agreements with the experiments have been suggested in earlier studies [22,27].

The uncertainties in these λ-scaling plots for results of the experiments (blue asterisks) and the *ab initio* models are indicated by horizontal error bars. Here, the uncertainty arises from the fact that two independent *ab initio*-model derivations give a slight difference ($\sim 5\%$) [3], together with the error caused by details of orbital variations ignored in the uniform λ scaling ($\sim 5\%$).

Quantum critical point of the AF transition appears at around ($\lambda \sim 0.95$). The overall agreement among the λ-scaled models, *ab initio* models, and the experiments show that the material dependence of the magnetism is well described by the variation of the correlation strength represented by the single parameter λ.

In addition to the interaction control, they may be substituted by other elements so that carriers are doped by holes or electrons (namely the filling control) as compared to the mother materials at d^6. This simultaneous possibility of the interaction and filling controls makes the iron-based superconductors valuable and unique in comparison to the cuprates (mainly, filling control only) or organic conductors (mainly, bandwidth control only) [28]. Furthermore, nearly degenerate five $3d$ orbitals enable us to examine

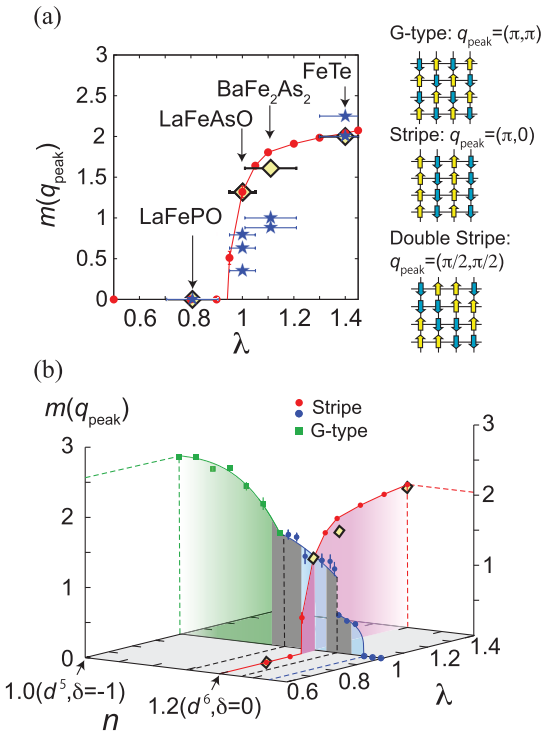

FIG. 1 (color). (a) Magnetic ordered moment $m(q_{\rm peak})$ at the Bragg wave number $q_{\rm peak}$ (for the pattern, see right) calculated by MVMC simulations (red circles). The result at $\lambda = 1$ represents that of the *ab initio* model for LaFeAsO while the λ dependence illustrates the results of the models obtained by uniformly scaling the interaction strengths by λ. The black-framed yellow diamonds indicate the results of the *ab initio* models, where they are plotted at the corresponding λ. The plotted results are those in the thermodynamic limit after the size extrapolation. Experimentally observed values [5–8] are also plotted at corresponding λ by asterisks, where FeTe shows double-stripe and others show stripe orders in agreement with our *ab initio* results. (b) Magnetic ordered moment in the plane of λ and doping concentration δ. The data are plotted in the cross sections for $\lambda = 1$ as well as for $\delta = 0$. It shows a peak at d^5 ($\delta = -1.0$) and decreases monotonically over d^6 ($\delta = 0$), which forms a large half-dome structure peaked at d^5. The MVMC results of the *ab initio* models are shown by black-framed yellow diamonds. The green and blue shaded regions represent the G-type and stripe-type AF orders, respectively, as is illustrated in the right panel of Fig. 1(a). There exist two first-order transitions (black dashed lines), one indicated by the jumps in the ordered moment around $\delta \sim 0.17$ and the other at the transition between the G-type and stripe around $\delta \sim -0.22$, which signals large charge fluctuations under phase-separation effects. In the present short-ranged-interaction model, the phase separation indeed occurs in the gray shaded regions.

multiorbital effects, that are absent in the cuprates and the organic conductors.

In the plane of λ as well as the doping concentration δ, the magnetic ordered moment $m(q_{\rm peak})$ is plotted in Fig. 1(b). Here, as in λ, δ monitors the doping effect, if the real material could be purely doped without changing other parameters such as the transfers. By this monitoring, we can elucidate physics of the filling control. As we clarify later, we caution that it does not simply mean the substitution effect of the real material, because the real substitution may change other parameters. Although the region near the d^5 configuration has not been experimentally realized so far, our monitoring of the filling control predicts that the iron-based superconductors around $\delta = 0$ (d^6) are located in the foot of a large dome centered at $\delta = -1.0$ (d^5). It was formerly believed that metallic "valleys" at noninteger fillings intervene the insulators formed at each integer filling (see for instance Fig. 65 of Ref. [24]). In marked contrast, the monotonic decrease in $m(q_{\rm peak})$ from d^5 over d^6 supports that the electron correlation of the iron-based superconductors around d^6 emerges just as a proximity effect of the d^5 Mott insulator without a good metallic region between d^5 and d^6 for the retained interaction strength. Ishida and Liebsch pointed out the strong correlation effect near d^5 in their single-site dynamical-mean-field study for a theoretical model, in terms of the "spin freezing" [29]. Our result indicates, instead of the spin freezing, that a big dome of antiferromagnetically ordered phase emerges, which was unable to be studied in their single-site study.

Indeed the orbital-resolved momentum distribution $n_\nu(k)$ in Fig. 2 shows that the clear jump manifested at the Fermi surface of good metals becomes less and less clear with decreasing electron concentration from d^6 ($\delta = 0$) toward d^5 ($\delta = -1$). The reason for the strong incoherence toward d^5 is that all the orbitals become nearly half filling at d^5. Such a strong commensurability leads to a solid Mott insulator. The large dome structure is a consequence of an overwhelming strong proximity of the d^5 (half-filled) Mott insulator, which blankets the d^6 commensurability. Furthermore, signatures of several first-order transitions seen in Fig. 1(b) in the filling control signal large charge fluctuations with tendency toward the phase separation and incoherence.

Another important aspect found in the doping dependence is the switching in the magnetic order, the transition from the stripe to G-type orders at $\delta \sim -0.22$ [Fig. 1(b)], which is explained by the geometrical frustration effects: The ratio of the diagonal next-nearest (t') to the nearest-neighbor (t) transfers, i.e., t'/t measures the frustration effect. In fact, d_{YZ}/d_{ZX} and $d_{X^2-Y^2}$ orbitals have $t'/t \sim 1.0$, while for d_{XY} and d_{Z^2} orbitals $t'/t \sim 0.1$ [3], where the orbitals are labeled in the representation of the folded Brillouin zone [3]. Around d^6, the frustrated $d_{X^2-Y^2}$ is dominant because of the differentiated pinning to half

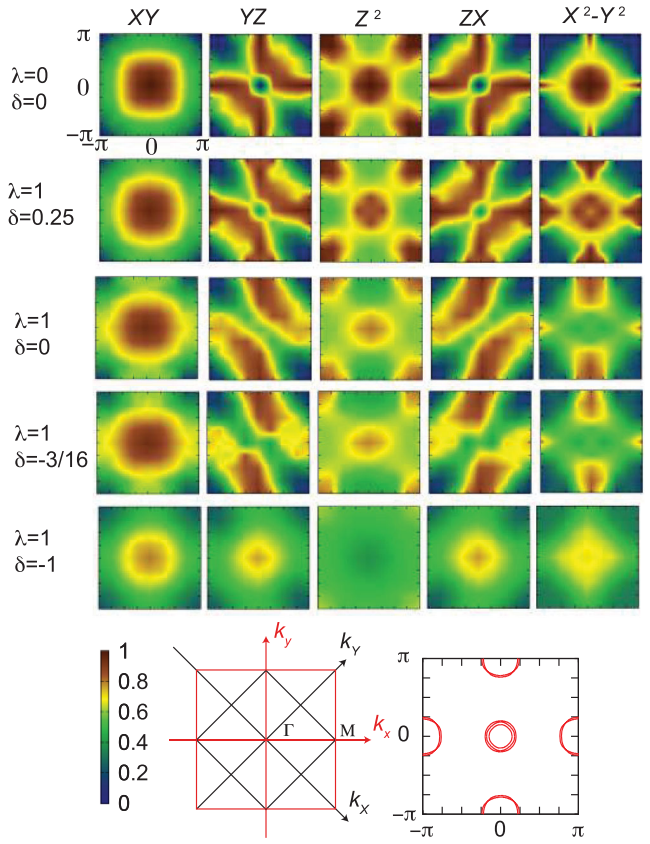

FIG. 2 (color). Filling dependence of orbital-resolved momentum distribution $n_\nu(k) \equiv \langle c^\dagger_{\nu,k} c_{\nu,k} \rangle$ plotted for the "unfolded" Brillouin zone (BZ), where the creation and annihilation operators of an electron at the orbital ν and the wave number k are denoted by $c^\dagger_{\nu,k}$ and $c_{\nu,k}$, respectively. In the bottom left, the unfolded BZ (with the coordinates k_x and k_y) and folded BZ (with k_X and k_Y) are depicted by the red and black lines, respectively. In the bottom right, the Fermi surfaces of the local density approximation band structures are shown by the red curve, which can be identified in the corresponding sharp changes in $n_\nu(k)$ for $\nu = d_{YZ/ZX}$ and $d_{X^2-Y^2}$ on the top panels. Note that the orbitals are represented according to the folded BZ. Fade out of sharp boundaries in $n_\nu(k)$, representing the Fermi pockets, are seen especially for $d_{YZ/ZX}$ and $d_{X^2-Y^2}$ together with d_{Z^2}, which signals strong renormalizations of quasiparticles with bad metallic behavior when δ decreases progressively to negative.

filling, while near d^5, all the orbitals are pinned to half filling and d_{XY} and d_{Z^2} become the more important players because of the larger effective interactions, which favors the G-type order. Nearby G-type order is suggestive of proposed nodes in the pairing symmetry of heavily hole doped KFe_2As_2 [30,31]. In this connection, the double-stripe-type order at $(\pi/2, \pi/2)$ experimentally observed for FeTe is also accounted for by the involvement of the less frustrated d_{Z^2} orbital.

To further understand the proximity effect of d^5 Mott physics, we monitor the effects of Coulomb (U)

and exchange (J) interactions separately by the scaling parameters λ_U and λ_J, respectively. Figure 3 reveals that U and J comparably contribute at d^6 in enhancing the ordered magnetic moment. The Hund's rule coupling J retains the metallic but AF order even far away from half filling (d^5) contrary to the quick collapse of the AF order in the cuprates. The present result conforms with a suggestion of an importance of J away from half filling [32]. We see below that J between $d_{X^2-Y^2}$ and d_{Z^2} orbitals is crucial in the iron families.

Around d^6, large spin and orbital fluctuations are prominent with the nearby magnetic quantum critical point. Figs. 3(b) and 3(c) illustrate that the $d_{X^2-Y^2}$ orbital is under the strongest correlation effects indicated by the smallest double occupation [panel (b)] and a remarkable pinning around half filling [(c)] even for relatively small λ, though the effective Coulomb interaction on the $d_{X^2-Y^2}$ is the smallest even at $\lambda = 1$ [25]; i.e., the onsite intraorbital interaction for the $d_{X^2-Y^2}$ orbital is 1.68 eV in comparison to 2.24–2.75 eV for other intraorbital values. (See Table I in [23].) This puzzle is solved by the largest bare density of states at the Fermi level (see Fig. 3 of Ref. [3]), which

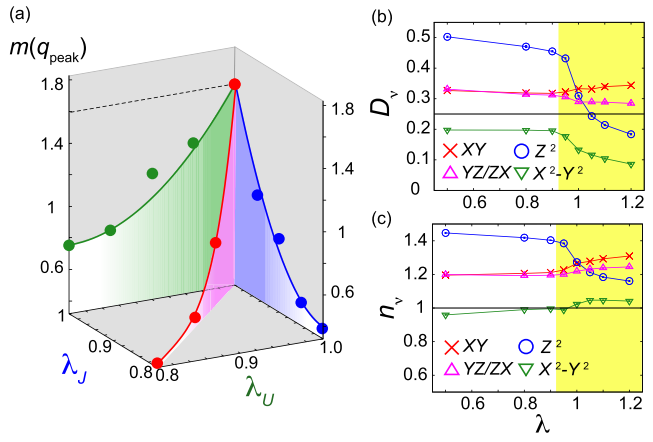

FIG. 3 (color online). (a) Magnetic ordered moments in the plane of λ_U and λ_J for system size $N_s = 6 \times 6$, which is expected to be close to the thermodynamic limit. Here, λ_J (λ_U) scales exchange (Coulomb) interactions from the *ab initio* model for LaFeAsO at $\lambda_U = \lambda_J = 1$. The sharp change in the ordered magnetic moment is triggered by a synergy effect of the direct Coulomb (λ_U) and the exchange (λ_J) interactions and the two interactions comparably contribute. (b) Orbital-resolved double occupation D_ν defined by probability of simultaneous occupation of up and down spin electrons on the ν orbital at the same site. (c) Orbital occupation n_ν defined by the averaged density of electrons on the orbital ν as a function of λ at filling $\delta = 0(d^6)$. Antiferromagnetic phase is represented as shaded region. System sizes 8×8 for (b) and (c) are sufficient to well represent these quantities in the thermodynamic limit. Near the realistic parameter $\lambda = 1$, strong correlation of the $d_{X^2-Y^2}$ orbital synergetically starts involving the d_{Z^2} orbital through the Hund's rule coupling, which drives the d_{Z^2} into the state close to half filling $n = 1$ with reduced D.

sensitively allows the electron correlation through the electron-hole polarizations. When λ increases around $\lambda = 1$ (realistic for LaFeAsO), the d_{Z^2} orbital quickly follows up the $d_{X^2-Y^2}$, because the $d_{X^2-Y^2}$ orbital has the largest Hund's rule coupling J with d_{Z^2} (0.43 eV in comparison to 0.23 eV with d_{XY} and 0.35 eV with $d_{YZ/ZX}$). The moment at the d_{Z^2} orbital grows, dragged by $d_{X^2-Y^2}$ through J. We confirmed that such orbital differentiations occur commonly in the *ab initio* models for other families [16]. The strong crossover from low to high magnetic moments by changing from LaFeAsO, $BaFe_2As_2$ through FeTe is accounted by this interplay of $d_{X^2-Y^2}$ and d_{Z^2} orbitals.

One might suspect that the disappearance of the magnetic order in hole doped $Ba_{1-x}K_xFe_2As_2$ at $x \sim 0.4$ [33] appears to contradict the present result. However, K doping does not work as a simple filling control but yields more complicated effects, because the Fe square lattice shrinks upon the K doping. This simultaneously enhances the bandwidth (nearly 10%) and works also as the bandwidth control driving into weak correlation regime. At $\delta = -1$ and $\lambda = 1$, we obtained the d^5 Mott insulator with a large Mott gap (~ 2.2 eV) with a high ordered moment ($\sim 2.5\mu_B$). It implies a connection with a G-type AF insulator in isostructural but d^5 compound LaMnPO [34].

Summary.—We have shown that the underlying proximity effects of the d^5 Mott insulator governs the electronic structures of iron-based superconductors, which are located around d^6 filling. When the Mott proximity is weakened, strong orbital and spin fluctuations take place before the verge to weakly correlated metals. This is indeed the high-T_c superconducting region around the d^6 filling. It shares a common character with the cuprates, while a new aspect here is an involvement of the orbital fluctuation and differentiation under the big umbrella of the d^5 Mott insulator. Although d^6 is commensurate filling, the Dirac nodes in the band dispersions maintain the metal for an unexpectedly wide region [22,35], while the interactions develop the antiferromagnetism. The AF quantum critical points accompany the strong crossover of the orbital polarization as well and the superconducting mechanism has to be clarified under this circumstance. We propose to focus particularly on the role of the $d_{X^2-Y^2}$ and d_{Z^2} orbitals as the leading players, in contrast to the d_{YZ}/d_{ZX} orbitals in the nesting picture. In the present results, the d^5 dominance washes away the subtlety of the nesting. Experimental clarification of the large dome structure in the full bandwidth and filling controls in the range from d^5 to d^6 is highly desired to clarify the whole perspective of the electron correlation effect in the iron-based superconductors.

The authors are indebted to Takashi Miyake for valuable discussions and providing us with his band structure data. They also thank Daisuke Tahara and Satoshi Morita for providing us with efficient MVMC codes. They are grateful to Toshiyuki Imamura for the usage of his matrix diagonalization code. This work is financially supported

by MEXT HPCI Strategic Programs for Innovative Research (SPIRE) and Computational Materials Science Initiative (CMSI). The authors thank Lawrence Livermore National Laboratory for generous offer of the supercomputer facilities. Numerical calculation was partly carried out at the Supercomputer Center, Institute for Solid State Physics, University of Tokyo. This work was also supported by Grant-in-Aid for Scientific Research (No. 22104010, No. 22340090, No. 22740215, and No. 23740261) from MEXT, Japan.

[1] Y. Kamihara, T. Watanabe, M. Hirano, and H. Hosono, J. Am. Chem. Soc. **130**, 3296 (2008).
[2] J. G. Bednorz and K. A. Müller, Z. Phys. **64**, 189 (1986).
[3] T. Miyake, K. Nakamura, R. Arita, and M. Imada, J. Phys. Soc. Jpn. **79**, 044705 (2010).
[4] For a review see, H. Hosono, Y. Nakai, and K. Ishida, J. Phys. Soc. Jpn. **78**, 062001 (2009).
[5] C. de La Cruz *et al.*, Nature (London) **453**, 899 (2008).
[6] N. Qureshi, Y. Drees, J. Werner, S. Wurmehl, C. Hess, R. Klingeler, B. Büchner, M. T. Fernández-Díaz, and M. Braden, Phys. Rev. B **82**, 184521 (2010).
[7] Q. Huang, Y. Qiu, W. Bao, M. A. Green, J. W. Lynn, Y. C. Gasparovic, T. Wu, G. Wu, and X. H. Chen, Phys. Rev. Lett. **101**, 257003 (2008).
[8] S. Li *et al.*, Phys. Rev. B **79**, 054503 (2009).
[9] A. V. Boris, N. N. Kovaleva, S. S. A. Seo, J. S. Kim, P. Popovich, Y. Matiks, R. K. Kremer, and B. Keimer, Phys. Rev. Lett. **102**, 027001 (2009).
[10] J. Yang, D. Hüvonen, U. Nagel, T. Rõõm, N. Ni, P. C. Canfield, S. L. Bud'ko, J. P. Carbotte, and T. Timusk, Phys. Rev. Lett. **102**, 187003 (2009).
[11] M. M. Qazilbash, J. J. Hamlin, R. E. Baumbach, L. Zhang, D. J. Singh, M. B. Maple, and D. N. Basov, Nature Phys. **5**, 647 (2009).
[12] L. Degiorgi, New J. Phys. **13**, 023011 (2011).
[13] T. Terashima *et al.*, J. Phys. Soc. Jpn. **79**, 053702 (2010).
[14] A. Tamai *et al.*, Phys. Rev. Lett. **104**, 097002 (2010).
[15] Y. Nakai, K. Ishida, Y. Kamihara, M. Hirano, and H. Hosono, J. Phys. Soc. Jpn. **77**, 073701 (2008).
[16] M. Aichhorn, S. Biermann, T. Miyake, A. Georges, and M. Imada, Phys. Rev. B **82**, 064504 (2010).
[17] W. Malaeb, T. Yoshida, T. Kataoka, A. Fujimori, M. Kubota, Y. Kahihara, M. Hirano, and H. Hosono, J. Phys. Soc. Jpn. **77**, 093714 (2008).
[18] W. L. Yang *et al.*, Phys. Rev. B **80**, 014508 (2009).
[19] M. Imada and T. Miyake, J. Phys. Soc. Jpn. **79**, 112001 (2010).
[20] C. Platt, R. Thomale, and W. Hanke, Phys. Rev. B **84**, 235121 (2011).
[21] D. Tahara and M. Imada, J. Phys. Soc. Jpn. **77**, 114701 (2008).
[22] T. Misawa, K. Nakamura, and M. Imada, J. Phys. Soc. Jpn. **80**, 023704 (2011).
[23] See Supplemental Material at http://link.aps.org/supplemental/10.1103/PhysRevLett.108.177007 for details of *ab initio* derivations of effective low-energy models, adequacy of single parameter scaling, and details of many-variable variational Monte Carlo method.
[24] M. Imada, A. Fujimori, and Y. Tokura, Rev. Mod. Phys. **70**, 1039 (1998).
[25] K. Nakamura, Y. Yoshimoto, Y. Nohara, and M. Imada, J. Phys. Soc. Jpn. **79**, 123708 (2010).
[26] K. Nakamura, R. Arita, and M. Imada, J. Phys. Soc. Jpn. **77**, 093711 (2008).
[27] Z. P. Yin, K. Haule, and G. Kotliar, Nature Mater. **10**, 932 (2011).
[28] K. Kanoda, J. Phys. Soc. Jpn. **75**, 051007 (2006).
[29] H. Ishida and A. Liebsch, Phys. Rev. B **81**, 054513 (2010).
[30] H. Fukazawa *et al.*, J. Phys. Soc. Jpn. **78**, 083712 (2009).
[31] K. Hashimoto *et al.*, Phys. Rev. B **82**, 014526 (2010).
[32] L. de'Medici, J. Mravlje, and A. Georges, Phys. Rev. Lett. **107**, 256401 (2011).
[33] H. Chen *et al.*, Europhys. Lett. **85**, 17006 (2009).
[34] J. W. Simonson, K. Post, C. Marques, G. Smith, O. Khatib, D. N. Basov, and M. C. Aronson, Phys. Rev. B **84**, 165129 (2011).
[35] Y. Ran, F. Wang, H. Zhai, A. Vishwanath, and D.-H. Lee, Phys. Rev. B **79**, 014505 (2009).